Iranian Journal of Science & Technology, Transaction B, Vol. 28, No. B2
Printed in Islamic Republic of Iran, 2004

TENSILE BEHAVIOR OF POWDER METALLURGY PROCESSED (Al-Cu-Mg-Mn) /SiC_p COMPOSITES*

I. UYGUR

Duzce Teknik Egitim Fakultesi, Abant Izzet Baysal Universitesi, 81620 Beciyorukler/Duzce, Turkey
E-mail: ilyasuygu@hotmail.com

Abstract – The tensile behavior of Al-Cu-Mg-Mn alloy matrix composites produced by a powder metallurgy process was investigated as a function of particle size and volume fraction in a naturally aged condition (T4). Microstructural examinations have enabled identification of particles and grain structure of the materials. The results indicated that tensile properties of the composites significantly improved in the yield strength, UTS and elastic modulus, on incorporation of hard, brittle ceramic particles as compared to unreinforced counterparts. On the other hand, ductility decreased considerably due to the brittle ceramic particles. The results were discussed in the light of microstructures.

Keywords – Composites, tensile behavior, 2124 Al-alloy, MMC, SiC_p

1. INTRODUCTION

High strength aluminium alloys (2000 and 7000 series) matrix composites reinforced by SiC particles are of great industrial interest due to the relatively lower cost and their ability to be processed by conventional methods. These composites are used for structural applications [1]. Al-alloys with SiC_p reinforced composites are attractive because of their enhanced tensile strength and stiffness, thermomechanical fatigue response, creep performance, excellent wear resistance, low thermal expansion and good corrosion resistance, and improved fatigue properties compared with unreinforced counterparts [2-7]. The tensile behaviour of MMCs is important for many applications. The tensile response of MMCs has been influenced by the following properties of the matrix alloy: reinforcement type (continuous, whisker or particulate) volume fraction of reinforcement, composition, heat treatment, and processing technique (casting or powder metallurgy) [8-11]. The role of the reinforcement particles are well understood in many studies, but there is no clear understanding of the effect of reinforcement particle size (P_z) and volume fraction (V_f) on the tensile response of the metal matrix composites. This particular study is mainly aimed at investigating the effect of P_z and V_f on the tensile properties of 2124 Al-Cu-Mg-Mn /SiC_p composites in naturally aged (T4) conditions.

2. MATERIALS AND EXPERIMENTAL PROCEDURE

The materials were commercial 2124 (Al-Cu-Mg-Mn) Al-alloys with 17 and 25 vol% with SiC particulate MMCs. All of the materials were produced by Aerospace Composite Materials (U.K) which were referred to as AMC217 (17 vol% 2-3μm SiC_p) AMC225 (25 vol% 2-3μm SiC_p), LAMC217 (17 vol% 10-20μm SiC_p), LAMC225 (25 vol% 10-20μm SiC_p) using powder metallurgy (P/M) processing. Prior to the machining process, a solution treatment was applied at 505 ^oC for 1 hour, followed by cold water quenching, and after that, natural ageing (T4) at room temperature for 100 hours. Tensile testing on MMCs was carried out on a computer controlled Instron servohydraulic test system. The alloy composition is given in Table 1. Typical

*Received by the editors March 12, 2002 and in final revised form January 1, 2003

micrographs of the composites are shown in Figs. 1a-e. Cylindrical hour glass shape specimens (6 mm diameter and 65 mm long gauge sections), were machined from the extruded bars. A 12.5 mm gauge length clip on an extensometer with ± 2.5 mm extension was used on the longitudinal direction of the specimens to monitor the strain. The tests were carried out at a strain rate of 6.7×10^{-4} s^{-1}.

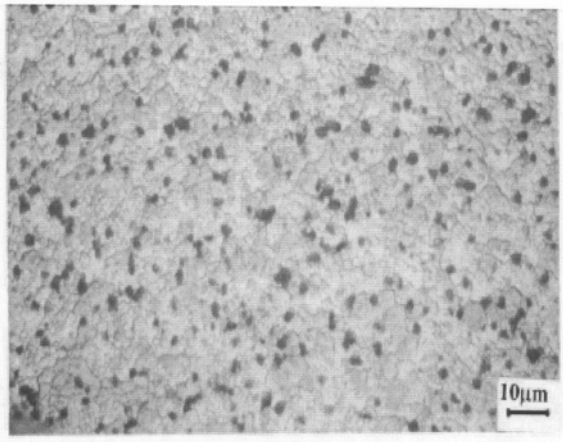

Fig. 1a. Microstructure of AMC200 unreinforced base alloy

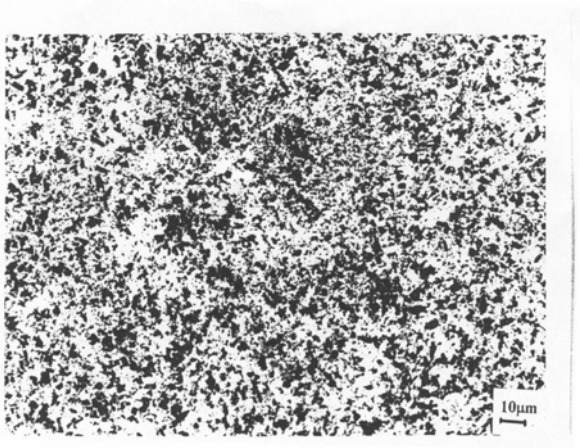

Fig. 1b. Microstructure of AMC217 particulate reinforced composite

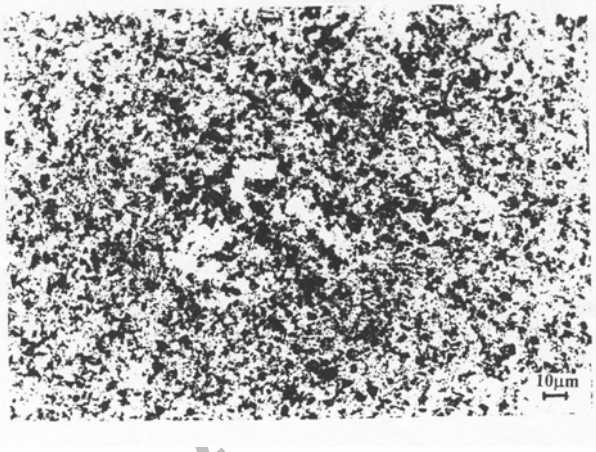

Fig. 1c. Microstructure of AMC225 particulate reinforced composite

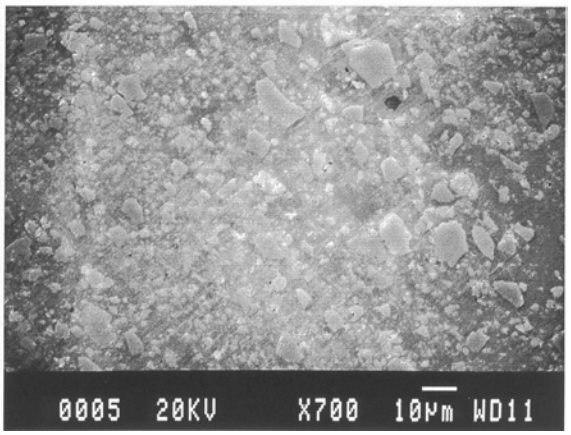

Fig. 1d. Microstructure of LAMC217 particulate reinforced composite

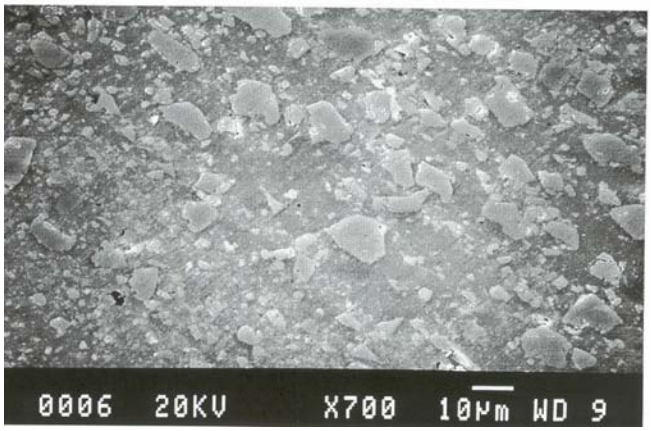

Fig. 1e. Microstructure of LAMC225 particulate reinforced composite

Table 1. Chemical composition of the composites

Element	Cu	Mg	Mn	Fe	Zn	Si	Cr	Others	Al
Weight %	4-4.4	1.3-1.6	0.5	0.3 max	0.25	0.2	0.1	0.45 total	Balance

Specimens for microscopic studies were prepared in the usual way by first grinding on emery papers followed by polishing on velvet cloth using diamond paste of <1μm fines. The characterisation of the grains and SiC particles was achieved using a Power Macintosh 7100/80 computer connected to a Reichert-JungMeF3 optical microscope. In order to examine the mechanism of the failure and the detailed microstructure, JEOL 35 c SEM was used.

3. RESULTS

a) Microstructure

Optical and SEM micrograph of unetched MMCs have been presented in Figs. 1a-e. No voids or regions of macroscopically clumped particles were found in the composite materials. Although the particle size in some of the alloy variants were as large as 28μm, there was no evidence of cracked or interfacial separation, indicating a well bonded interfacial structure. The distribution of particles in MMCs produced by P/M routes are relatively uniform on the macroscopic scale. It is generally argued that SiC_p distribution is important because micro crack nucleation and coalescence in the composite are highly dependent on local V_f rather than on an average value for the whole material [12]. The microstructure of the alloys also revealed that there were some coarse and fine intermetallic particles inside the matrix alloy. BE analysis of these particles demonstrated that they contained Cu, Mg, Fe, Si, Mn, and Al. They probably originated during the casting of the master alloy ingots used in the P/M processing. In analogy to other related reports, it is believed that the larger constituents were $Cu_2Mn_3Al_{20}$, $FeCu_2Al_7$, and $CuMnAl_2$ [13], while smaller particles were Manganese containing dispersoids $Al_{20}Cu_2Mn_3$ [14].

Quantitative metallographic examinations indicated that the fine SiC_p composites had a more uniform distribution than the coarsed particulate composites. The average particle size (D), minimum particle size (D_{min}), maximum particle size (D_{max}), the aspect ratio ($D_{max\,/\,min}$), standard deviations (SD), and measured V_f are given in Table 2.

Table 2 . Geometric characteristics of SiC particles

Materials	D(μm)	D_{max}(μm)±SD	D_{min}(μm)±SD	Aspect ratio	Measured SiC_p(%)	Fabricated SiC_p(%)	Sizes(μm)
LAMC225	14.7	26±1.1	8.1±2.1	3.21	26	25	10-20
LAMC217	16.4	29.8±3.6	9.6±3.9	3.1	17	17	10-20
AMC225 Transverse	1.95	4.5±0.65	0.14±0.1	32.4	28	25	2-3
AMC225 Longidition	2.18	5.8±0.73	0.35±0.3	16.5	27	25	2-3
AMC217	2.6	7.89±2.4	0.65±0.3	12.13	19	17	2-3

A comparison of the measured V_f with a given value is slightly different. This is probably caused by many different types of small intermetallics which were examined using LAMC217 and AMC225 composites. Figure 2a is a SEM picture of the LAMC217 microstructure and Fig. 2b is [SEM backscaterred] picture of the same material. It is evident from the backscattered electron (BE) images in these figures that all the MMCs as well as unreinforced alloy, contain a high density of intermetallic particles. BE analysis of the white particles which were ≤1μm, gave an average chemical composition of Fe (1.91%), Cu (8.8%), Si (5.41%), and Mg (7.6%). Both coarse and fine particles can be seen in Fig. 2b. These intermetallic inclusions are most likely to have precipitated during vacuum hot pressing, solidification or the extrusion process [15]. The dark particles were SiC on compositions Si (54.89%) and C (44.21%). Similar studies

were carried out for etched LAMC225-T4 material. The BE picture is shown in Fig. 3. Intermetallic particles have significantly larger dimensions than the LAMC 217 material. Their average dimension was 2 μm with some as large as 6 μm.

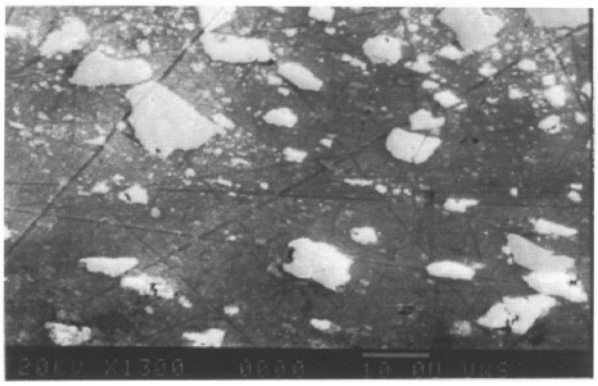

Fig. 2a. SEM micrograph of LAMC217 composite material

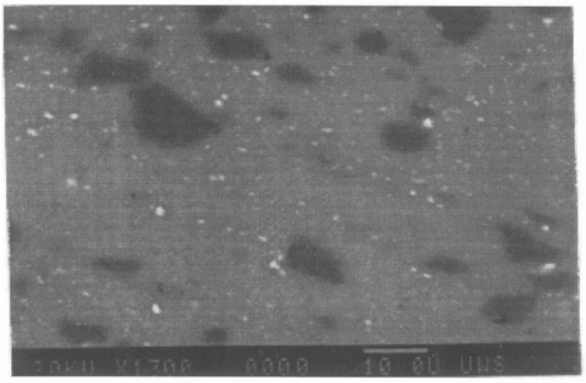

Fig. 2b. Back scattered (BE) SEM picture of LAMC217

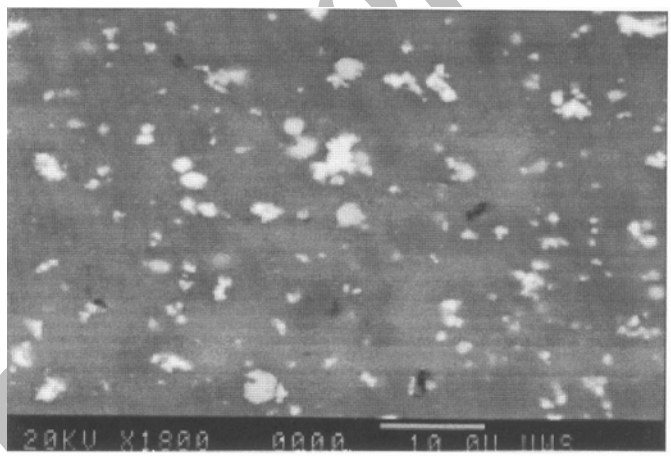

Fig. 3. Back scattered (BE) SEM picture of LAMC225

Table 3 gives a comparison of the general chemical composition of alloys as measured from the BE analysis. The subscript "m" and "s" indicate measured and specified values, respectively. Although the measured and specified average values are different in some cases, overall similar values were obtained.

Table 3. Chemical composition Al-alloy MMCs

Materials	Cu_s%	Cu_m%	Mg_s%	Mg_m%	Mn_s%	Mn_m%	SiC_s%	SiC_m%
AMC225	3.85	3.49	1.5	1.2	0.6	0.55	25	24.6
LAMC217	4	3.76	1.3	0.98	0.4	0.36	17	17.5

The P/M processed AMC200 base material was polished and etched with Keller's reagent to allow measurement of grain size on transverse and longitudinal sections. The optical microscopy picture is given in Fig. 4. Polished surfaces did not reveal clear grain structures, but intermetallic particles were readily apparent and located at grain boundaries. The mean linear intercept (MLI) method was used to measure the grain sizes [16]. The results are recorded in Table 4. It is evident that the average grain size is significantly reduced by heat treatment (T4). Longitudinally sectioned grains were larger in size than transversed ones. The grains were flattened and elongated parallel to the extrusion direction, as a consequence of the deformation process.

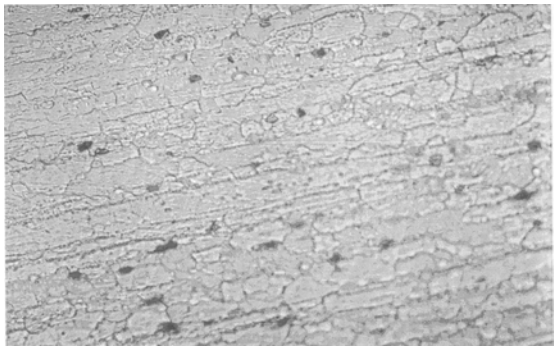

Fig. 4. Grain structure of AMC200 base alloy (longitudinal section)

Table 4. Grain size measurement of base AMC200-T1 and T4 material

Condition	Total measurement	Maximum grain size (μm)	Minimum grain size (μm)	Measured total grains	Average grain size (μm) ± SD
T1- Transverse	15	14.75	7.4	100	10 ± 3
T1- Longitudinal	10	22	9.2	80	14 ± 3.7
T4- Transverse	70	10.5	4	243	8.5 ± 1.2
T4- Longitudinal	47	20.6	7	182	13.5 ± 4

b) Hardness test

The Vickers hardness results are listed in Table 5 for the various alloys, as received (T1) and solution treated, aged (T4) conditions. The hardness of heat treated (T4) composites compared with (T1) condition increased, but the amount depends on the P_z and V_f of the reinforcement particles. In all cases, increasing V_f and P_z resulted in higher hardness values. Presumably a higher dislocation density and higher hardness of the SiC particles are responsible for the enhancement over the base alloy. The intense dislocation density is generated during water quenching from the T4 treatment as a result of the large difference in the coefficient of the thermal expansion between Al and SiC particles. These hardness values of the composites correspond to high values of elastic modulus and yield strength compared to the base alloy. The hardness of the T4 composites are significantly increased compared with the T1 condition.

Table 5. Vickers hardness results for the MMCs and base alloy (AMC200) in the T1 and T4 conditions

Materials	Volume fraction (%)	Nominal particle Size (μm)	Condition	Vickers hardness (Kgf/mm^2)
AMC200	-	-	T1	132
AMC200	-	-	T4	145
AMC217	19	2.6	T4	193
LAMC217	17	16.4	T4	220
AMC225	28	1.95	T1	225
AMC225	28	1.95	T4	243
LAMC225	25	14.7	T4	250

c) Tensile properties of MMCs

A representative true stress against true strain is shown in Fig. 5 for AMC217 and AMC225 materials. The yield strength (σ_{YS}), the ultimate tensile stress (σ_{UTS}), Young's modulus (E), and strain to failure (ε_f) were calculated from this plot and the values are listed in Table 6.

Table 6. Tensile properties of the composites and base alloy in the T4 condition

Materials	P_z (μm)	V_f (%)	Matrix	E (GPa)	σ_y (MPa)	σ_{UTS} (MPa)	ε_f (%)	Density
AMC217	2.6	19	2124	111	375	680	7.2	2.85
AMC225	2	28	2124	142	400	692	4.3	2.85
Base Alloy*	-	-	2124	72	325	470	11	2.77

*Results were taken from producer data sheet

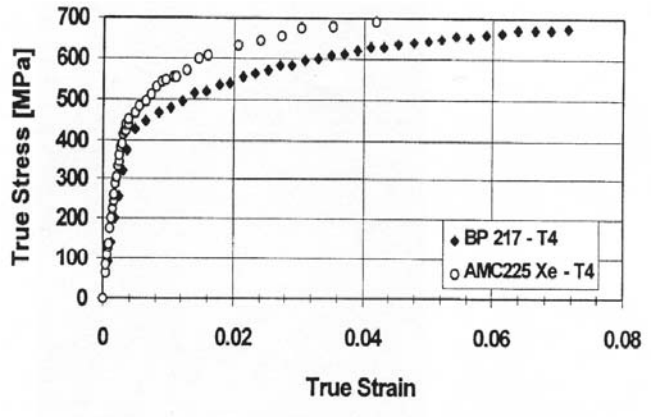

Fig. 5. Stress-strain response of AMC217 and AMC225 composites

The V_f of the SiC_p was found to have a significant effect on the tensile properties of both MMCs. The modulus, yield strength and the UTS of the composites are dramatically enhanced with respect to the unreinforced base alloy. The AMC225 material has a Young's modulus greater than 140 GPa. However, the improvement of these properties is associated with a reduction in strain to failure (monotonic tensile ductility). Furthermore, for a constant P_z, an increase of V_f from 17 vol% to 25 vol% resulted in dramatic reduction of the monotonic ductility from 7.2 % to 4.3 %.

It is well established that [17] the following yield stress-strain data can be represented by simple power law

$$\sigma = K\,(\varepsilon)^n \tag{1}$$

where K is the strength coefficient and "n" is the strain hardening exponent. A log-log plot of true stress-strain results in a straight line if Eq. (1) applies. For most metals, "n" has value in the range of 0.1-0.5 [17]. The log-log monotonic stress-strain curves and coefficient are shown in Fig. 6 for both MMCs. It is clearly seen that both values increase with increasing V_f of reinforcement particles.

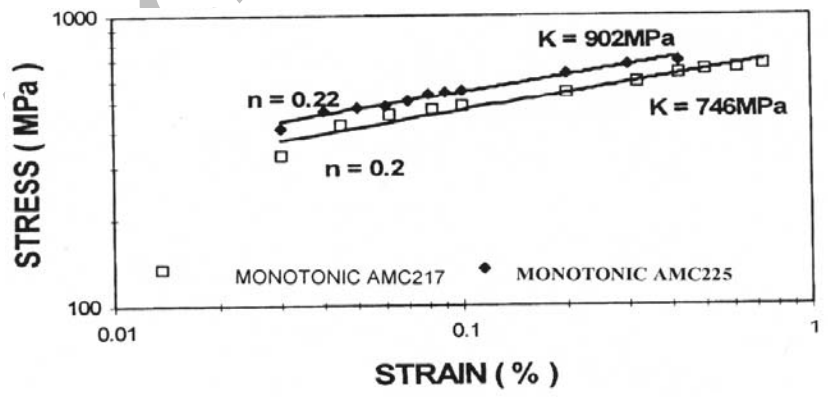

Fig. 6. Monotonic Log-Log stress-strain curve of the composites

b) Tensile fractography

Typical SEM micrographs of the tensile fracture surface of naturally aged AMC225 composite material are shown in Figs. 7a-d. Although the composite exhibited very limited ductility on a macroscopic scale, SEM micrographs suggest that fracture occurred in a ductile manner. The presence of intermetallic constituents caused very fine shallow dimples, while coarser and much deeper equiaxed dimples were associated with the SiC_p. Both are indicative of a predominantly ductile failure process (Fig. 7c). The crack initiation region was unclear and featureless. There were no obvious defects that suggest very good microstructural properties (Fig. 7b). No fractured reinforcement particles were observed on the fracture surfaces of the composite containing 2μm SiC_p (Fig. 7d).

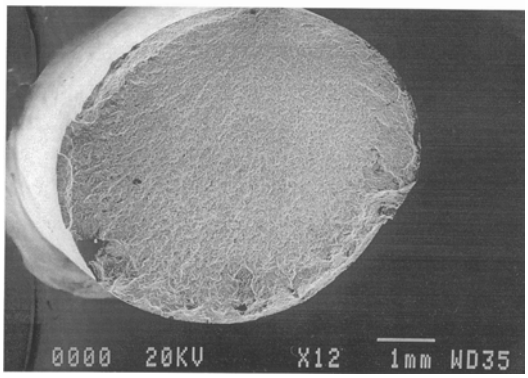

Fig. 7a. SEM picture of fractured tensile specimen of AMC225 composite

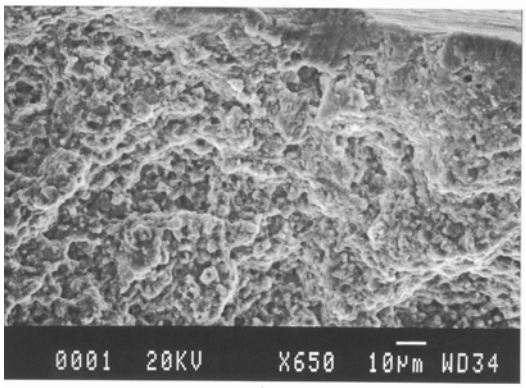

Fig. 7b. High magnification SEM image of initiation region

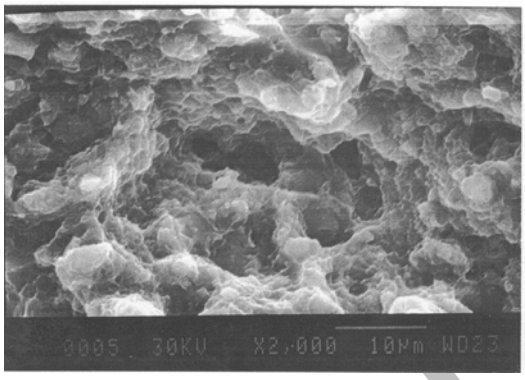

Fig. 7c. SEM micrograph of the same material, showing very fine and coarse dimples on the fracture surface

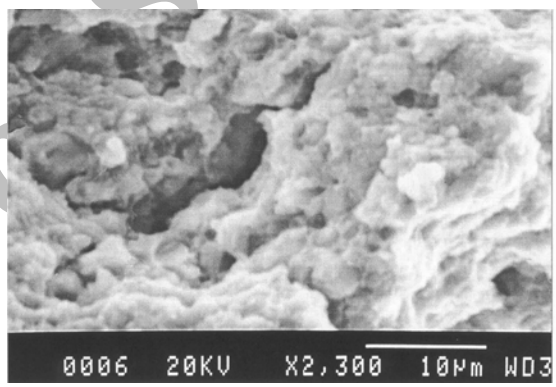

Fig. 7d. SEM picture of fracture surfaces, showing falt cleavage of SiC_p interfaces and propagation of microcrack from the interfaces into the base alloy

4. DISCUSSION

a) Microstructure

Distribution of SiC particles strongly affects the mechanical properties of the MMCs. As shown in Fig.1a, through Fig.1e, the distribution of SiC_p becomes more inhomogeneous as the SiC_p size increased. Thus, the fine reinforcement particulate composites AMC217 and AMC225 have a uniform microstructure compared to the coarse reinforced variants. The effect of microstructure on mechanical properties of the 2xxx Al-SiC_p composites has been extensively discussed in Ref. [18].

In this study, the composites demonstrated a reasonable uniform distribution of SiC_p in the 2124 matrix alloy with good interfacial bonding between particles and matrix alloy. It is known that P/M processing, unlike alternative techniques such as casting, rarely results in reactant on the interface, thereby promoting excellent interfacial bonding [19]. The microstructure also appears to be void free, which confirms there has been complete densification during the hot-pressing operation. The previous work [21] examination of the fracture surfaces showed that the fatigue crack initiation regions were usually associated with coarse SiC_p, large SiO_2 particles or large intermetallic constituents. Similar crack initiation behaviour in MMCs has been observed previously [7, 19, 20]. It was reported that [22] coarse intermetallic particles were potential void nucleation regions and that the voids linked to each other during the fatigue process. These large defects appear to have a stress raising effect which leads to the formation of slip bands and then fatigue cracks.

The size and distribution for intermetallic particles contribute to the sequence of events leading to fracture [13]. As an example, coarse Mn-containing dispersoids played an important role in controlling fracture resistance, since the voids formed at the larger constituent particles were linked through the

secondary void formation at dispersoids [14]. Alternatively, very fine Mn-dispersoids act as barriers to the dislocation motion promoting cross-slip, which leads to a uniform homogenous deformation. Consequently, crack initiation is delayed and the fatigue life is extended compared to an Al-alloy without the Mn dispersoids [23].

In the present study, the average grain size was 6.5μm on transverse sections and 12μm on longitudinal sections for the 2124 base alloy in the T4 condition. The average grain size for the composites can be calculated by the following formula [24]:

$$\text{Grain Size} = P_z\,[(1-V_f)/V_f]^{1/3} \tag{2}$$

The calculated grain size is 5μm for the AMC217, 4μm for the AMC225, 27μm for the LAMC217, and 20μm for the LAMC225. It was reported [14] that in the 2124+17vol% 2-3μm SiC_p (AMC217), the average grain size is 6μm in the longitudinal section and 4μm in transverse section. Similarly, Wu and Lavernia [25] showed that the grain size of MMCs decreased with increasing the V_f of reinforcement particles. In their case, grain size of unreinforced material was around 34 μm, while the grain size of 6061 5 vol% SiC_p was 22 μm. The decrease in grain size is probably due to pinning by the SiC particles.

b) Tensile response of materials

The results of the tensile tests presented in the results section show that the addition of SiC_p causes an increase in the Yield strength, UTS and modulus of the 2124-T4 MMCs. Although the tensile response of LAMC217 and LAMC225 composites were not evaluated, their yield strength and Young Modulus (E) could be obtained from the first cycle stress-strain loop of the R=0 strain control fatigue tests [21]. These results are given in Table 7.

Table 7. Mechanical properties of all variants obtained by strain controlled fatigue tests (R=0)

Materials	Condition	$E_{measured}$ (GPa)	$E_{calculated}$ (GPa)	Yield strength (MPa)
LAMC225	T4	122	128	475
LAMC217	T4	108	109	397
AMC225	T4	130	128	497
AMC225*	T4	116	-	500
AMC217	T4	109	109	418
AMC217*	T4	100	-	400

*Results were taken from manufacturers data sheet.

McDanels [7] studied a variety of Al-alloy composites with V_f ranging from 10 to 40 pct and found that the increase in the modulus was less than had been predicted by the rule of mixtures (ROM). The results obtained in the present study are also significantly lower than ROM when 400 GPa and 72 GPa are taken as a modulus for the SiC and for base alloy, respectively. The E values of modulus lay within the upper bound [154GPa] and lower bound [91GPa] as calculated using Eq. (3) and (4) [27, 28]:

$$\text{Upper bound (ROM)} \quad E_c = E_m V_m + E_r V_r \tag{3}$$

$$\text{Lower bound} \qquad E_c = E_m \frac{E_m V_m + E_r (V_r + 1)}{E_r \cdot V_m + E_m (V_r + 1)} \tag{4}$$

where the subscripts “c”, “m”, and “r” refer to the composite, the matrix, and the reinforcement, respectively. The calculated average values of these two equations are very close to the measured values (see Table 7).

The reinforcement particles affect the tensile properties for a variety of reasons, such as the high dislocation density at matrix/particle interface [26, 29]. The dislocation density ρ may be estimated as follows [2]:

$$\rho = 12\Delta T \Delta C \frac{V_f}{bP_z} \tag{5}$$

where ΔT is the temperature change, ΔC is the mismatch in coefficient of thermal expansion between matrix and SiC_p. V_f and P_z are the volume fraction and particle size of reinforcement particles, respectively and "b" is the Burger vector. For the alloy system used in this study, the value of "b" is 0.165 nm, ΔT is 470K, ΔC is $19.2.10^{-6}$ K^{-1} and V_f is 0.17 and 0.25 calculated values of the composites are summarized in Table 8.

Table 8. Calculated dislocation density for the experimental materials

Composite	Average Particle Size (μm)	ρ m^{-2}
AMC217	2.6	$4.3 .10^{10}$
LAMC217	16.4	$6.8 . 10^{9}$
AMC225	2.5	$6.5 . 10^{10}$
LAMC225	14.7	$1.11 . 10^{10}$

It is evident that AMC225 containing a fine and high volume fraction of SiC_p has the highest dislocation density. The amount of dislocation generation is affected by CTE, particle size, particle-volume fraction, and matrix strength [30]. Also particle spacing, reduced grain size and formation of subgrains in the matrix affect dislocation motion which affects the tensile response of composites. The strain hardening is the idea that dislocations pile-up on slip planes at barriers in the crystal. The pile-ups produce a back stress which opposes the applied stress on the slip plane. Microscopic precipitate and foreign particles can serve as barriers, thus the composite (AMC225) with higher particle-volume fraction shows a higher strain hardening exponent than the composite (AMC217) with a lower particle-volume fraction (Fig. 6).

Moreover, the following constituent features strongly affect the mechanical response of MMCs. a) Reinforcement type (whisker, particulate, continuos fibre), b) Alloy composition, c) Reinforcement content d) Heat treatment, e) Processing techniques, f) Reinforcement size. The effect of V_f and P_z on elastic modulus and yield strength of the 2124 Al-alloy composites are presented in Table 7 for the present study. Homogenization heat treatment produces very fine Guinier-Preston (GP) zones that are sheared by the movement of dislocations such that matrix deforms by planar slip. The yield stress increases with increasing particle volume fraction. At any given particle-volume fraction, the composites with smaller particles exhibit higher strength than the composites with larger particles. The fine particulate reinforced MMCs had advantages including, higher UTS, higher E, better ductility, easier machining, and better distribution of particles compared to the coarse particulate 2124 Al-alloy MMCs.

5. CONCLUSIONS

1. There is a substantial increase in yield strength, elastic modulus and UTS of the MMCs with respect to their unreinforced counterparts. The observed improvement is attributed to the generation of higher dislocation density in the matrix of all MMCs because of the thermal mismatch between the matrix and SiC reinforcement.
2. For a given heat treatment (T4) with an increase in V_f and P_z, an increase in hardness values in the composite materials results.
3. Tensile fracture occurs in a ductile manner with related fine and coarse dimples in fracture surface.

Acknowledgement: The Author thanks Prof. Dr. W.J. Evans and Dr. M. R. Bache at The University of Wales, Swansea for their great assistance. The work described here was carried out in the Department of Materials Engineering at University of Wales, Swansea.

REFERENCES

1. Goni, J., Mitxelena, I. & Coleto, J. (2000). Development of low cost MMCs for commercial applications, *Mater. Sci & Tech., 16*, p.743.
2. Varma, V. K., Kamat, S. V. & Kutumbarao, V. V. (2001). Tensile behavior of P/M processed (al-Cu-Mg)/SiCp composites. *Mater. Sci. & Tech., 17*, 93.
3. Sehitoglu, H. & Karakaya, M. (1990). Thermomechanical fatigue of Al-SiC_p composites. *Proceeding of the 4th International Conference in "Fatigue" Honolulu* (Ed. H. Kitagawa and T. Tanaka), 163.

4. Ma, Z. Y. & Tjong, S. C. (2001). Creep deformation characteristics of discontinuously reinforced MMCs. *Composite Science and Tech., 61*(5), 771.
5. Zhang., X. M., Man, H. C. & Yue, T. M. (1996). Corrosion properties of excimer laser surface treated Al-SiC MMC. *Scripta Mater., 35*(9), 1095.
6. Bonnen, J. J., Alisson, J. E. & Jones, J. W. (1991). Fatigue behavior of a 2xxx series aluminum alloy reinforced with 15vol% SiCp. *Metal. Trans*., *22A*, 1007.
7. McDanels, D. L. (1985). Analysis of stress-strain fracture and ductility behavior of Al-matrix composites containing discontinuously SiC reinforcement. *Metall. Trans., 16A,* 1105.
8. Pinto, I. & Zschech, E. (1996). Mechanical properties and corrosion behavior of extrusions for aircraft applications made by discontinuously SiCp reinforced MMCs. *Materials Sci. Forum, 217-222*, 1593.
9. Manson, J. J. & Ritchie, R. O. (1997). Fatigue crack growth resistance in SiCp and whisker reinforced P/M 2124 Al-matrix composites. *Mater. Sci. &Eng., A231*, 170.
10. Shakesheff, A. J. (1995). Aging and toughness of SiCp reinforced Al-Cu and Al-Cu-Mg based MMCs. *J. of Mater. Sci., 30*, 2269.
11. Sugimura, Y. & Suresh, S. (1992). Effects of SiC content on fatigue crack growth in Al-alloys reinforced with SiCp. *Metall. Trans., 23A*, 2231.
12. Thomson, D. S. (1975). Microstructural and mechanical characteristics of MMCs. *Metall. Trans. 6A*, 671.
13. Srivatsan, T. S., Lanning, D. Jr. & Koni, K. K. (1993). Microstructure, tensile properties and fracture behavior of an Al-Cu-Mg aloy 2124. *J. Mater. Sci., 28*, 3205.
14. Srivatsan, T. S., Lanning, D. Jr. & Koni, K. K. (1993). Cyclic strain resistance and cyclic fracture behavior of 2124 Al-alloy. *Int. J. Fatigue, 15*(3), 231.
15. Zong, Y. & Derby, B. (1993). Microstructure and fracture behavior of SiCp-Al-2618 MMC. *J. De Physique, II*(3), 1861.
16. Pickering, F. B. (1976). *The basic of quantitative metallography*. Institute of Metallurgy Technicians, U.K.
17. Dieter, G. E. (1988). *Mechanical metallurgy*. McGraw-Hill Book Comp. Ltd. U.K.
18. Shin, K., Chung, D. & Lee, S. (1997). The effect of consolidation temperature on microstructure and mechanical properties in P/M processed 2xxx Al-alloy composites reinforced with SiCp. *Metall. Trans., 28A*, 2625.
19. Davidson, D. L. (1993). Fatigue and fracture toughness of Al-alloys reinforced with SiC and alumina particles. *Composites, 24*(3). 248.
20. Yu, W., Wang, J. & Wang, Z. (1990). Fatigue behavior of SiC_p Al-6061 composite. *Proceeding of the 4th International Conference in "Fatigue" Honolulu* (ed. H. Kitagawa and T. Tanaka), 899.
21. Uygur, I. (1999). Environmentally assisted fatigue response of Al-Cu-Mg-Mn with SiC particulate metal matrix composites. Ph. D thesis University of Wales, Swansea, U.K.
22. Llorca, J. J., Suresh, S. & Needleman, A. (1992). An experimental and numerical study of cyclic deformation in MMCs. *Metall. Trans., 23A*, 919.
23. Kim, K. C. & Nam, S. W. (1998). Effects of Mn-dispersoids on the fatigue mechanism in Al-Zn-Mg alloy. *Mater. Sci. & Eng., A244*, 257.
24. Brown, C. W. (1992). Particulate MMC properties. BP Research, 203.
25. Wu, Y. & Lavernia, E. J. (1991). Spray aotomised and codeposited 6061 Al/SiCp composites. *Journal of Metallurgy, 16*, 1.
26. Thomas, M. P. & King, J. E. (1994). The effect of long-range thermal residual stress fields on fatigue crack growth in Al-SiCp MMCs and their measurement by neutron diffraction. *J. Mater. Sci., 29*, 5272.
27. Stone, I. C. & Tsarkirpolous, D. (1998). The effect of reinforcement on the notched and unnotched room temperature tensile properties of Al-4wt%Cu/SiCp MMCs. *Mater. Sci.&Eng., A241*, 19.
28. Ress, D. W. A. (1998). Deformation and fracture of MMCs under combined loadings. *Composites, 29A*, 171.
29. Jacquesson, M., Vidal-Setif, M. H., Valle, R., Godin, N., Girard, A. & Faugeres, R. (2000). Fatigue behavior of Al-matrix composites reinforced with continuous alumina fibres. *Mater. Sci. & Tech., 16*, 830.
30. Kim, C. T., Lee, J. K. & Plichta, M. R. (1990). Plastic relaxation of thermoelastic stress in Al-ceramic composites. *Metall. Trans., 21A*, 613.